Available online at www.sciencedirect.com
ScienceDirect
Journal of the European Ceramic Society 28 (2008) 2983–2993
www.elsevier.com/locate/jeurceramsoc

Abrasive wear of Al_2O_3–SiC and Al_2O_3–(SiC)–C composites with micrometer- and submicrometer-sized alumina matrix grains

Jaroslav Sedláček [a,b,*], Dušan Galusek [b], Peter Švančárek [b], Ralf Riedel [c], Alan Atkinson [d], Xin Wang [d]

[a] *Institute of Ceramics in Mechanical Engineering, University of Karlsruhe, Haid-und-Neu-Str. 7, Karlsruhe D-76131, Germany*
[b] *Vitrum Laugaricio—Joint Glass Centre of the Institute of Inorganic Chemistry, Slovak Academy of Sciences, Alexander Dubček University of Trenčín, and RONA, j.s.c., Študentská 2, Trenčín 91150, Slovak Republic*
[c] *Institute of Materials Science, Darmstadt University of Technology, Petersenstrasse 23, Darmstadt D-64287, Germany*
[d] *Department of Materials, Imperial College London, Exhibition Road, London SW7 2AZ, United Kingdom*

Received 26 January 2008; received in revised form 16 April 2008; accepted 18 April 2008
Available online 24 June 2008

Abstract

The response of Al_2O_3, Al_2O_3–SiC–(C) and Al_2O_3–C nanocomposites to grinding was investigated in terms of changes of quality of ground surfaces and of the weight losses with time. The study used monolithic polycrystalline aluminas as references, and alumina-based composites with nanosized SiC and C inclusions and with alumina matrix grain size varying from submicrometer to approximately 4 μm. The studied materials can be roughly divided into two groups. Materials with submicrometer alumina matrix grains (Group 1) wear predominantly by plastic deformation and grooving. Coarse-grained materials (Group 2) wear by mixed wear mechanism involving crack initiation and interlinking accompanied by grain pull-out, plastic deformation and grooving. The wear rate of composites increases with increasing volume fraction of SiC. The Group 2 materials wear much faster then those with submicron microstructure. In all cases (with one exception) the wear resistance of composites was higher than that of pure aluminas of comparable grain sizes used as reference materials.

Keywords: Al_2O_3–SiC; Al_2O_3–(C); Precursors—organic; Microstructure—final; Mechanical properties; Wear resistance

1. Introduction

The wear resistance of polycrystalline alumina shows a large variability, depending on the characteristics of the material such as grain size, sintering aids and residual porosity. Therefore, the wear rates can differ from one material to another significantly. The grain size dependence of wear of alumina was studied by Miranda-Martinez et al.[1] who found a decrease in wear of alumina with decreasing grain size. The grain size dependence of wear of alumina was explained by Davidge and Riley, who attributed the mass loss to microcrack initiation, propagation, and coalescence, which finally led to grain detachment. Cracks propagate by a "stop and go" mechanism: a crack propagates at constant rate along grain boundaries with stops for readjustment of the direction of crack propagation at triple grain boundary junctions. If the grain size is smaller, the crack encounters triple junctions more frequently and the overall rate of crack propagation is lower.[2] However, this mechanism does not explain the grain size dependence of wear of liquid phase-sintered aluminas, or alumina-based composites (e.g. Al_2O_3–SiC), which are known to wear, depending on conditions applied, by transgranular fracture, plastic deformation/grooving, or tribochemically.[3]

The published data on wear of Al_2O_3–SiC nanocomposites and the monolithic alumina of the same grain size and under the same testing conditions report more than three times higher erosion resistance[4–6] and reduction of dry sliding wear rate[7] of composites with respect to the monolithic alumina with comparable grain size. Addition of SiC nanoparticles into polycrystalline alumina produces a noticeable improvement in surface quality during lapping and polishing.[8–10] This is considered to be the result of a reduction of grain pullout during grinding and polishing, which in turn, is believed to be

* Corresponding author at: Institute of Ceramics in Mechanical Engineering, University of Karlsruhe, Haid-und-Neu-Str. 7, Karlsruhe D-76131, Germany. Tel.: +49 721 608 4247; fax: +49 721 608 8891.
E-mail address: uachjase@savba.sk (J. Sedláček).

0955-2219/$ – see front matter © 2008 Elsevier Ltd. All rights reserved.
doi:10.1016/j.jeurceramsoc.2008.04.018

the consequence of altered way of fracture from intergranular in monolithic alumina, to transgranular in nanocomposites.[11] There exist various explanations for the observed change of the fracture mode, ranging from the strengthening of grain boundaries,[12,13] and crack deflection from grain boundaries into the interior of alumina grains by thermal residual stresses around intragranular SiC particles,[14] through changes in surface flaw population, to the presence of surface residual stresses.[15] Todd and Limpichaipanit recently suggested that the role of SiC in nanocomposites with high SiC volume fractions (10 vol%) is in suppression of brittle fracture of alumina by blocking the formation of long twins and dislocation pileups, which are thought to be responsible for crack initiation by intragranular SiC particles (i.e. a form of slip homogenisation). They also suggest that the reason for the observed change of fracture mode from intergranular in monolithic alumina to transgranular in SiC-containing composites (including those with added micrometer-sized SiC particles) can be sought in the change of the system's chemistry, rather than in purely mechanical interactions between alumina and SiC.[16] However, there exists no general agreement on which mechanism is responsible for the observed changes in mechanical and wear properties of "nanocomposites", and it remains unclear whether the SiC particles inside the alumina grains or those at the grain boundaries are primarily responsible for these changes.

The lack of general agreement on these issues is often the result of differences in sample preparation, and conditions applied during the wear test. In this work we therefore prepared a range of composite materials with various alumina matrix grains size, and volume fraction of SiC and focused on a particular wear mode – abrasion – under defined conditions. This paper investigates the wear behaviour of various aluminas and alumina-based composites with 3–8 vol% SiC, in some cases containing also residual free carbon, with special focus on the influence of various material's parameters (the mean size of alumina matrix grains, size and distribution of nanoparticles, and the fraction of residual porosity), and the mechanical properties (hardness, fracture resistance), as measured by Vickers indentation, on abrasive wear.

2. Experimental

The details on composition and preparation of all studied materials are summarized in Table 1. All alumina samples and alumina-based nanocomposites were prepared from the α-alumina powder Taimicron TM DAR (Taimei Chemicals Co., Ltd., Tokyo, Japan) with the mean particle size 150 nm.

2.1. Monolithic aluminas

Monolithic aluminas, both solid and liquid phase sintered were prepared as reference materials. The pure alumina references, hereafter denoted as T1 and T2, were prepared by uniaxial pressing of the alumina powder in a steel die at 100 MPa, followed by pressureless sintering at 1350 °C for 1 h in air. The sample T2 was subsequently annealed for 11 h at the same temperature in order to induce grain growth. Both the heating and cooling rates were 10 °C/min.

The liquid phase-sintered specimen denoted TCS5 was prepared by mixing the isopropanol suspension of the alumina powder with isopropanol solution of calcium nitrate $Ca(NO_3)_2{\cdot}4H_2O$ (AnalaR grade, BDH Ltd., Poole, UK) and tetraethylorthosilicate (TEOS, AnalaR grade, BDH Ltd., Poole, UK). Powder suspensions were homogenized for 2 h in a plastic jar with alumina milling balls, and an aqueous solution of ammonium hydroxide (10 wt.%) was then added to precipitate calcium hydroxide, and to hydrolyze the TEOS. The calcia-to-silica molar ratio was set to 0.2, in accord with our previous results, which indicate excellent wet erosive wear resistance of polycrystalline aluminas of this composition.[17] A further 1 h mixing at room temperature was allowed for completion of hydrolysis, and the suspension was then dried under an infrared lamp. The dry powder was calcined for 60 min at 700 °C and passed through a 100 μm mesh nylon sieve to provide a reasonably free-flowing powder. The powder was densified by hot pressing in a graphite die at 1450 °C and 20 MPa pressure for 10 min. The dilatometric measurement has shown that the conditions applied allowed for nearly complete densification.

2.2. Al_2O_3–C and Al_2O_3–SiC–(C) composites with submicrometer alumina matrix grains

Both the pure alumina powder and the powder with the composition TCS5 were freeze granulated in order to obtain a powder suitable for industrial-scale pressing. Each powder was granulated with a specific combination of commercial additives, later referred to as granulation additives, which allowed preparation of stabilized suspension with the lowest possible content of water. The suspension of the pure alumina powder was prepared with only 23 wt.% of distilled water with addition of 1.8 wt.% of an acrylate binder, 0.6 wt.% of the dispersant Dolapix CE64, and 1.5 wt.% of Zusoplast lubrication aid. The TCS5 powder required more water (38 wt.%) in order to achieve required fluidity. 2 wt.% of the acrylate binder, 1.6 wt.% Dolapix A88 dispersant, and 1.5 wt.% of Zusoplast lubrication aid were added. The suspensions were then ball milled for 20 h to ensure sufficient homogeneity, sprayed into liquid nitrogen and freeze-dried for 25 h. The granulated powders were sieved in order to obtain the fraction between 0.1 and 0.4 mm.

The granulated powders (denoted hereafter as TGHP and TCS5G) were pressed uniaxially in a steel die at 100 MPa and then hot pressed at the pressure of 30 MPa and the temperature of 1450 °C under vacuum. Densification was monitored by dilatometry, and the process was interrupted as soon as no further shrinkage was observed (after approximately 10–15 min under the conditions applied). The hot pressed samples were homogeneously black throughout the bulk due to the presence of residual carbon from the used organic additives. The content of residual carbon was determined by thermogravimetry of pulverized specimens in oxidation environment in the temperature range 20–1000 °C at the heating rate of 10 °C/min using the TG/DTA analyzer SDT 2960 (T.A. Instruments). In order to estimate the influence of residual carbon on mechanical proper-

Table 1
Composition and processing conditions

Name	Composition	Sintering conditions
T1	Al_2O_3	1350 °C/1 h, pressureless sintering, air
TGFS	Al_2O_3 + granulation additives	1350 °C/1 h, pressureless sintering, air
TGHP	Al_2O_3 + granulation additives	1450 °C/15 min, 30 MPa, hot pressing, vacuum
TCS5	Al_2O_3 + 5 wt.% $CaO{\cdot}5SiO_2$	1450 °C/20 min, 30 MPa, hot pressing, vacuum
TCS5G	Al_2O_3 + 5 wt.% $CaO{\cdot}5SiO_2$ + granulation additives	1450 °C/10 min, 30 MPa, hot pressing, vacuum
T2	Al_2O_3	1350 °C/1 h pressureless sintering + 1350 °C/11 h annealing, air
IP3	Al_2O_3 + 3 vol% SiC	1850 °C/3 h, pressureless sintering, Ar
IP5	Al_2O_3 + 5 vol% SiC	1850 °C/3 h, pressureless sintering, Ar
IP8	Al_2O_3 + 8 vol% SiC	1850 °C/3 h, pressureless sintering, Ar
IP8HIP	Al_2O_3 + 8 vol% SiC	1850 °C/3 h, pressureless sintering, Ar + HIP 1700 °C/2 h, 150 MPa

ties and wear the granulated alumina powder was densified also by free sintering under the same conditions as the specimen T1 so that all residual carbon from granulation aids was burned out in the process. The specimens prepared by pressureless sintering are hereafter denoted as TGFS.

2.3. Al_2O_3–SiC composites

The pure alumina powder was pressed axially in a steel die at 50 MPa and then isostatically at 500 MPa in order to prepare pellets with the diameter of 12 mm and of 6 mm height. The alumina green bodies were pre-sintered in air in an electrical furnace (HTM Reetz GmbH., Berlin, Germany, model LORA 1800) at 1160 °C without isothermal dwell in order to ensure sufficient handling strength, and to maintain the open porosity at the level allowing penetration of the infiltrant into the body. Liquid poly(allyl)carbosilane SMP-10 (StarFire Systems, Watervliet, NY) was used as the source of SiC. A single infiltration with concentrated polymer was required to obtain the composite with 8 vol% SiC (denoted as IP8). The composites with 3 and 5 vol% SiC (IP3 and IP5, respectively) were prepared by single infiltration with the polymer dissolved in appropriate amount of water-free cyclohexane (Sigma–Aldrich, Steinheim, Germany). After infiltration the solvent was evaporated by evacuating the samples for 2 h at room temperature. The specimens were then pyrolysed and pressureless sintered in Ar atmosphere in an electrical furnace with graphite heating elements at 1850 °C and with 3 h isothermal dwell at the maximum temperature. A powder bed containing 50 wt.% of Al_2O_3, 25 wt.% of SiC and 25 wt.% of carbon (soot) were added in order to prevent specimen decomposition and mass loss. Around 1000 °C the polymer transforms directly to amorphous SiC with high ceramic yield (75–80 wt.%), which then at higher temperatures crystallizes to β-SiC. The polymer decomposition (pyrolysis) is accompanied by evolution of hydrogen and of small amounts of hydrocarbons. The pyrolysis yields virtually no free carbon.[18] A sintered specimen of the IP8 composition was further hot isostatically pressed for 2 h at 1700 °C and 150 MPa (IP8HIP) in order to eliminate the residual porosity. The conditions were as mild as possible to eliminate the residual porosity, and at the same time not to induce the grain growth.

2.4. Characterization

The densities of all specimens were determined by Archimedes' method in mercury. The microstructures were examined by scanning electron microscopy (Philips XL30, Philips, Eindhoven, The Netherlands and Zeiss, model EVO 40 HV, Carl Zeiss SMT AG, Germany) on polished and chemically (composites, 5 min in concentrated H_3PO_4 at 230 °C), or thermally (monolithic aluminas, 4 h at 1100 °C) etched cross-sections of sintered specimens. Grain size was defined as 1.56 times mean linear intercept.

Mechanical properties, i.e. hardness and fracture resistance were estimated from Vickers indentations of polished specimens at the maximum indentation loads of 10 and 100 N, respectively. The fracture resistance was calculated from the length of radial cracks extending from the corners of the indents by the method described by Anstis.[19]

For a wear test Al_2O_3 and composite samples were mounted separately on a brass holder and ground using a flat bed grinder (Dap-7, Struers, Ballerup, Denmark) under the following conditions: 25 cm diameter metal bonded 120-grit diamond wheel; grinding wheel speed of 250 rpm; 50 N load on specimen. After 10 min the test was interrupted, the specimens were unmounted, washed in ethanol and dried at 100 °C for 1 h, and the weight loss by grinding was determined. The procedure was repeated six times in order to obtain the weight loss-time dependence for each specimen. Water, which also continually removed the grinding debris, was used as cooling liquid. Minimum of two tests were carried out for each material. The ground surfaces of tested specimens have been examined by SEM. The wear tests have been carefully controlled with respect to ensure the same condition and reproducibility for each specimen and all tests by using presureless-sintered Al_2O_3 as a reference material and by precise positioning both of specimen and reference material during the test.

In selected specimens the residual thermal stresses were mapped. A Raman optical microprobe (Renishaw model 2000, Renishaw, Gloucestershire, UK) employing incident radiation from a He/Ne laser with a photon wavelength of 633 nm was used to obtain Cr^{3+} photoluminescence spectra from polished cross-sections of tested specimens. Mapping was done over a relative small area of 100 μm × 100 μm using a laser spot size of

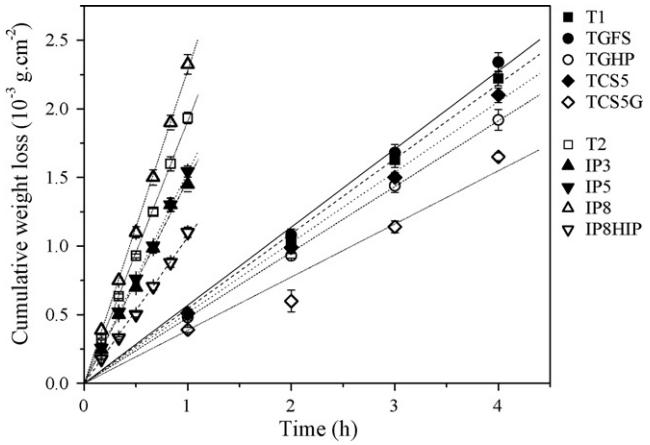

Fig. 1. Cumulative weight loss of monolithic aluminas and nanocomposites as a function of grinding time.

about 1.5 μm. After background subtraction the luminescence spectra were fitted to two Lorenzian–Gaussian peaks without application of any constraint. A sapphire single crystal was used as the stress free reference.

3. Results and discussion

Abrasive wear of all materials expressed in terms of cumulative weight loss during grinding is presented in Fig. 1. The tested materials can be quite obviously divided into two different groups. Group 1 comprises all materials (be it the composites or monolithic aluminas) with submicrometer microstructure and with higher wear resistance. Monolithic aluminas from the Group 1 (samples T1 and TGFS) wear faster than the corresponding composites (samples TCS5G and TGHP), or liquid phase-sintered monoliths (TCS5). Group 2 of materials comprises the nanocomposites from the set IP and the monolithic alumina T2 with the mean grain size of around 2 μm and more, which all wear comparatively faster than the Group 1 materials. Also in this case the monolithic alumina wears faster than most composites.

The wear rates were calculated from the weight loss-time dependences of respective samples by fitting the measured data with a straight line with the intercept equal to zero. The measured wear rates, together with other materials' properties are summarized in Table 2.

3.1. Mechanical properties and wear

Nearly 30 years ago it has been postulated that wear rate of ceramics is controlled by hardness and especially by its fracture toughness. Generally, a material with high hardness and with high fracture toughness should wear at a lower rate than a material that is less hard or one that has lower fracture toughness; the fracture toughness was considered to be a primary parameter to relate to the wear loss.[20] However, in wear processes of polycrystalline alumina ceramics the fracture occurs on the scale of individual grain size or less, microcracks propagate along the grain boundaries of individual grains, resulting in grain dislodgement and pull-out.[21] Fracture toughness values measured by macroscopic extension of crack do not therefore represent the type of fracture that occurs during wear process. At small crack size the microcracks tend to propagate preferentially in regions where the grain boundaries are under tension, effectively reducing the intrinsic grain boundary toughness. However, the deleterious effect of the internal stresses at small crack size is compensated by the countervailing influence of the bridging elements at large crack length. Thus, in the region of the greatest pertinence to wear process (i.e. small crack length) the resistance to crack extension is at its minimum. This minimum is strongest in the materials with the maximum large-crack toughness.[22] Similarly, the requirement of high hardness as a prerequisite for high abrasive wear resistance of hard ceramics has been questioned by Roberts.[23] The depths of cracks produced by hard abrading particles in ceramic counterfaces were found to decrease with decreasing counterface hardness. For soft counterfaces, the load applied to the surface being abraded may fall below the minimum required to cause any indentation fracture, thus completely eliminating the loss of material by crack formation and grain pull-out. Any direct relationship between the wear resistance and mechanical properties of hard polycrystalline materials is therefore questionable.

This presumption was confirmed by the results obtained in this study. The indentation fracture resistance of composites studied in this work is only moderately higher compared to the corresponding monolithic alumina samples. The mea-

Table 2
Properties of monolithic alumina ceramics and alumina-based composites

Name	Density (g cm^{-3})	D_{50} (Al_2O_3, μm)	D_{50} (SiC_{intra}, μm)	D_{50} (SiC_{inter}, μm)	Porosity (%, estimated)	H_{V1} (GPa)	K_{Ic} (MPa m$^{1/2}$)	Wear rate (μm h^{-1})
T1	3.920	0.8	–	–	1.5	20.3 ± 0.6	4.5 ± 0.1	1.4
TGFS	3.900	1.0	–	–	2.0	19.9 ± 0.3	4.9 ± 0.1	1.5
TGHP	3.814	0.6	n.m.	n.m.	2.1	23.1 ± 0.4	5.3 ± 0.1	1.3
TCS5	3.814	0.7	–	–	0.3	18.6 ± 0.3	5.0 ± 0.3	1.3
TCS5G	3.799	0.5	n.m.	n.m.	1.9	21.5 ± 0.7	4.6 ± 0.1	1.0
T2	3.932	2.2	–	–	1.2	18.3 ± 0.4	3.8 ± 0.7	4.9
IP3	3.887	4.0	196	n.m.	2.3	18.9 ± 0.2	4.6 ± 0.2	3.8
IP5	3.880	1.9	78	124	2.2	19.6 ± 0.8	4.3 ± 0.2	4.0
IP8	3.857	2.0	77	154	2.1	20.9 ± 0.7	4.8 ± 0.2	5.9
IP8HIP	3.869	2.0	n.m.	n.m.	1.4	21.1 ± 0.6	4.8 ± 0.1	2.8

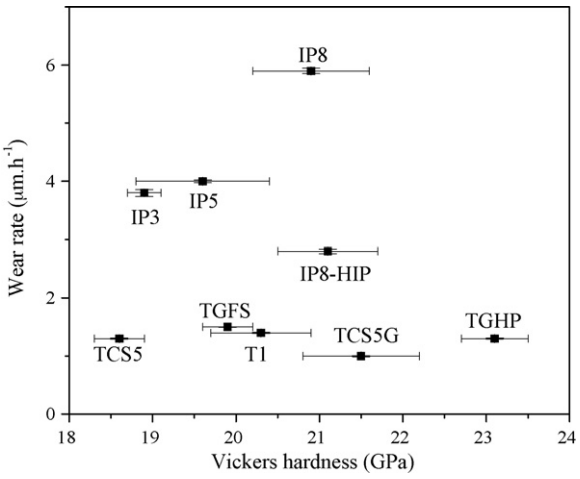

Fig. 2. Wear rates of monolithic aluminas and alumina-based composites vs. Vickers hardness.

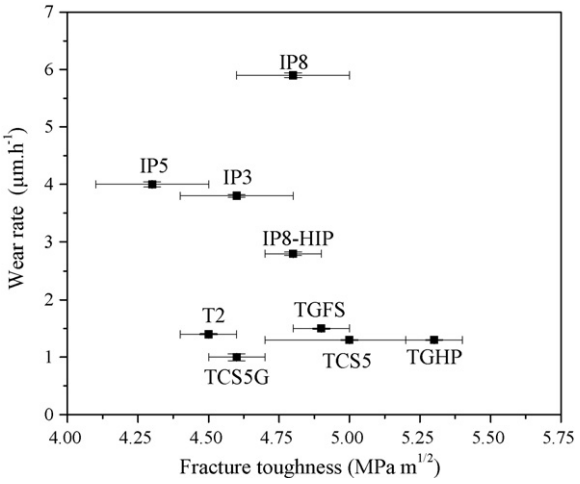

Fig. 3. Wear rates of monolithic aluminas and alumina-based composites vs. indentation fracture resistance.

surements also indicate only small influence of grain size, or composition on the fracture resistance (Table 2). The most pronounced effect is a moderate increase of fracture resistance of the Group 2 nanocomposites in comparison to the monolithic alumina with comparable grain size. The dispersion of C and/or SiC nanoparticles in Group 1 materials does not affect fracture resistance significantly. On the other hand, the hardness of the liquid phase-sintered monolithic alumina sample TCS5 (18.6 GPa) was markedly lower than that of the nanocomposite TGHP (23.1 GPa). In case of IP samples the hardness increased moderately with increasing volume fraction of SiC (Table 2). The relations between the wear rates and hardness and indentation fracture resistance of the studied materials are shown in Figs. 2 and 3, respectively. Apparently, the studied materials can be again divided into two groups – one including the materials with submicrometer microstructure, the second with the size of alumina matrix grains >1 μm. At comparable hardness, or fracture resistance, all Group 2 materials wear much faster than those in Group 1. Moreover, the wear rates of Group 1 materials do not depend on macroscopic mechanical properties. The wear resistance of the Group 2 pressureless-sintered samples seems to decrease with increasing hardness of the composites, which is in agreement with the conclusions drawn by Roberts.[23] No obvious trend between fracture resistance and wear of the Group 2 materials was observed. Interesting is the behaviour of the specimens IP8 and IP8HIP: both materials contain the same amount of SiC, they have virtually identical microstructures and macroscopic mechanical properties. The only obvious difference is the post-sinter HIP treatment of the IP8HIP, which resulted in small decrease of residual porosity from 2.1 to 1.4 vol%. However, IP8 wears twice as fast as IP8HIP. This indicates that the macroscopic mechanical properties are not the controlling parameter of wear, and that there must exist some other, not obviously apparent, mechanisms, which influence the wear behaviour: these will be discussed in the following sections.

3.2. Group 1 materials with submicrometer alumina matrix grains

The microstructure of each material in Group 1 consisted of equiaxed alumina matrix grains with various grain sizes, ranging between 0.5 and 1.0 μm (Table 2). Different grain size is the result of different sintering schedule, consolidation technique or the presence of second phase inclusions. Monolithic aluminas consist of equiaxed grains with narrow size distribution (Fig. 4a). The microstructure of composites with submicrometer alumina matrix grains was studied in detail previously.[24] The matrix grains of the composites TGHP and TCS5G are smaller

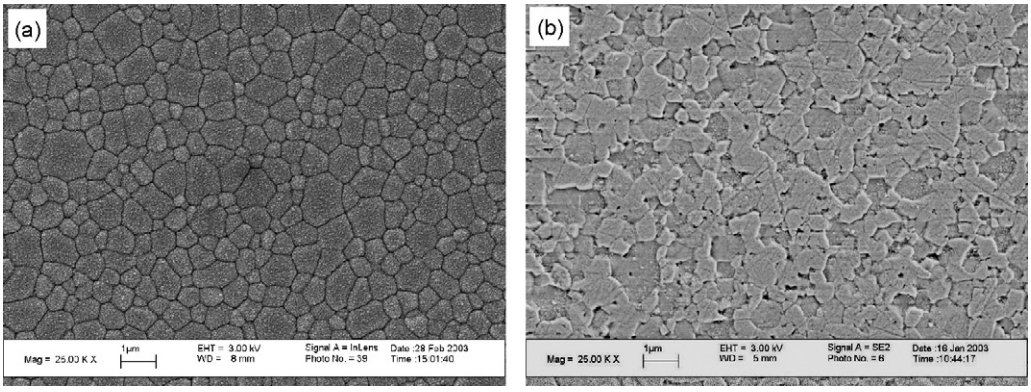

Fig. 4. Microstructure of thermally etched monolithic alumina – sample T1 (a) and of the chemically etched alumina–carbon nanocomposite – sample TGHP (b).

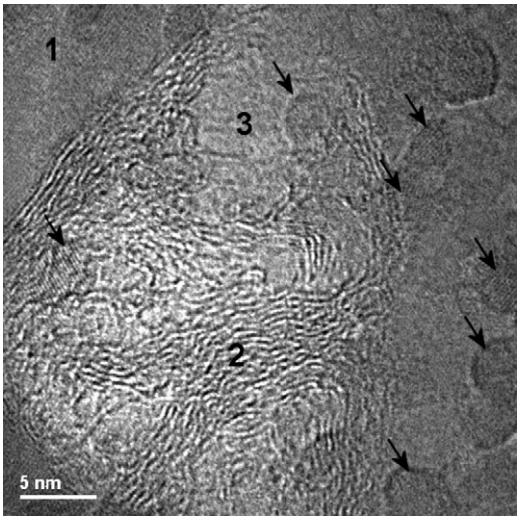

Fig. 5. The bright field TEM micrograph of the TCS5G sample (1, alumina grain; 2, turbostratic carbon; 3, aluminosilicate glass). The SiC inclusions are marked by arrows between.

than in monolithic alumina due to the presence of second phase inclusions at grain boundaries, which hinder grain growth by grain boundary pinning, Fig. 4b, and also due to much shorter sintering times (albeit higher temperatures) facilitated by the use of pressure in the course of densification. The carbon inclusions are formed by pyrolytic decomposition of organic species from granulation additives. In case of the sample TGHP the inclusions comprise only carbon particles located both within alumina grains and at Al_2O_3–Al_2O_3 grain boundaries. Similarly, pyrolytic carbon is created in TCS5G sample, but here also nanometer-sized SiC particles with diameter of about 30 nm are formed by *in situ* carbothermal reduction of deliberately added silica (Fig. 5).[24]

The apparent grain size–wear rate dependence in the Group 1 materials is shown in Fig. 6. The materials with finer microstructure have higher wear resistance and exhibit a monotonous relationship between wear rate and the grain size.

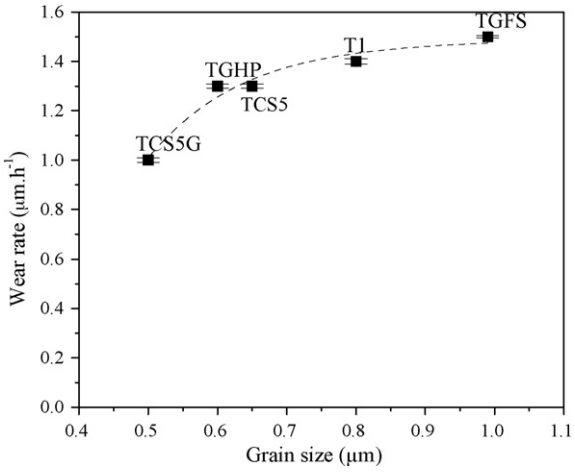

Fig. 6. Wear rate as a function of size of alumina matrix grains for monolithic alumina and for nanocomposites with submicrometer matrix grains.

Fig. 7 shows typical morphologies of wear surfaces of submicrometer monolithic aluminas (samples T1 and TCS5), Al_2O_3–C (TGHP), and Al_2O_3–SiC–(C) (TCS5G) nanocomposites. The ground surface of the monolithic alumina T1 shows clear evidence of grain pullout due to the intergranular fracture, which is responsible for mass loss during wear (Fig. 7a). Intergranular fracture is characteristic also for the TGFS where the carbon residua from granulation aids were burnt out during sintering.

Only limited and mostly transgranular fracture was observed in case of the sample TGHP, Fig. 7b, with occasional pits, most likely as the result of fracture at the sites of processing flaws. Grooved morphology of wear surfaces is the result of plastic deformation of the nanocomposite. The morphology of wear surface of the sample TCS5G, Fig. 7c, also indicates material removal mechanism controlled by plastic deformation with only occasional grain pull-out. Interestingly, the same applies for the monolithic, liquid phase-sintered alumina TCS5, where the wear is controlled by plastic deformation without any observable grain pull-out.

The observed wear features and likely mechanisms responsible for the change of fracture mode, suppression of fracture and tendency to plastic grooving are discussed below.

In monolithic aluminas tensile microstresses develop locally at grain boundaries because of thermoelastic anisotropy of alumina crystals. Especially triple junctions are often believed to be under significant tension and to act as microcrack nucleation sites. These are responsible for predominantly intergranular fracture in pure alumina, and also for mass loss during wear by initiation of intergranular microcracks at the places with the highest tensile stress, their propagation and coalescence. Although by their nature grain size invariant, the grain boundary microstresses were found to be smaller in finer grained monolithic aluminas due to easier relaxation by grain boundary diffusion than in their coarser grained counterparts: the initiation of grain boundary microcracking is therefore more difficult in fine grained materials, and the extent of grain pull-out during wear is diminished.[25] Grinding of alumina also results in extensive accumulation of lattice defects at grain boundaries. The larger are the grains, the greater is the dislocation density within the pile-ups and therefore higher stress concentration at grain boundaries, favouring the more extensive grain pull-out in coarser-grained materials.[26]

The relation between stresses and fracture in nanocomposites is not clear. Some theoretical works suggest that thermal residual stresses are the reason for the change of fracture mode in nanocomposites from intergranular to transgranular. These are supposed to develop during cooling from the sintering temperature due to the difference of thermal expansion of alumina matrix grains and of the second phase inclusions. However, the theories often contradict each other, they are not quantitative, or rely on special arrangement of nanoparticles to achieve desired strengthening effect: there also exists no general agreement concerning the role of intragranular SiC particles and the SiC particles at grain boundaries in crack propagation and deflection from grain boundaries into the matrix grains. When putting the numbers into reasoning, the Niihara's idea of

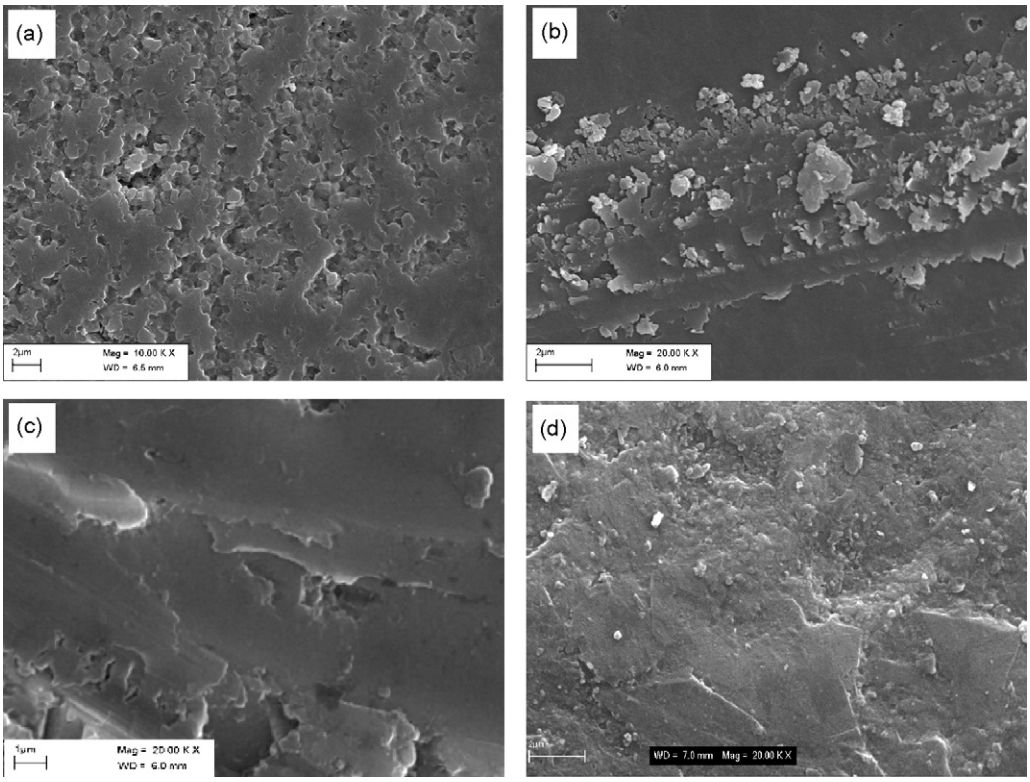

Fig. 7. Morphology of ground surface of pure monolithic alumina – sample T1 (a), the Al_2O_3–C nanocomposite – sample TGHP (b), Al_2O_3–SiC–(C) nanocomposite – sample TCS5G (c), and of the liquid phase-sintered monolithic alumina TCS5 (d).

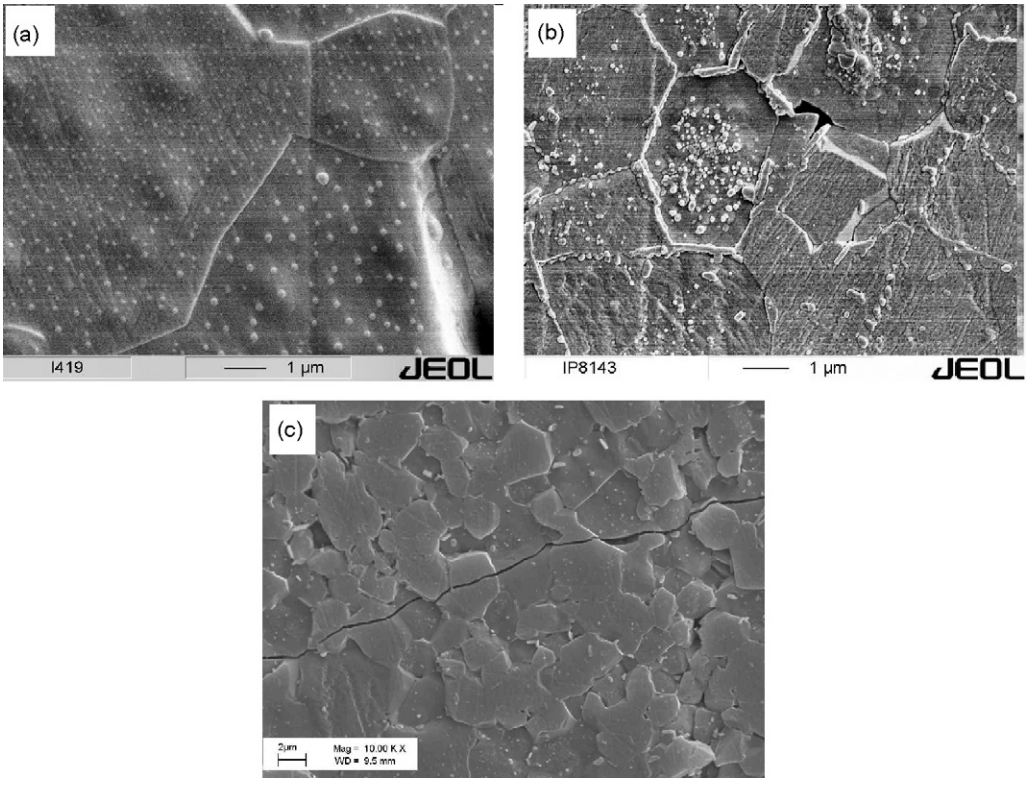

Fig. 8. Microstructures of alumina–silicon carbide nanocomposites: IP3 (a), IP8 (b), and IP8HIP (c). Brighter spots in alumina grains and at Al_2O_3–Al_2O_3 grain boundaries are the SiC nanoinclusions. The crack in (c) follows predominantly transgranular path.

intragranular SiC particles attracting cracks from the grain boundary into grains turns out to be weak. Any "nanoparticle effect" is small due to small distances that the stresses fluctuate over. The tensile residual stress from intragranular SiC inclusions that could cause spontaneous transgranular cleavage of alumina grains would require the SiC particle size of about 10 μm[27] whereas the size of particle in 'nanocomposies' is usually at the level of several tens of nanometers. Any significant weakening of alumina grains by the presence of intragranular SiC nanoparticles therefore seems unlikely. Moreover, some authors observed the change of fracture mode in Al_2O_3–SiC composites irrespective of the size and location of SiC particles, which they attributed to chemical, rather than a mechanical effect.[16] Various chemical interactions as the result of different origin and purity of used powders as well as different routes of preparation might therefore in part explain the contradictory results obtained by various authors. The observed change of fracture mode from inter- to intra-granular in calcium and magnesium silicate containing liquid phase-sintered aluminas, although in our original work attributed to the presence grain boundary strengthening thermal stresses, seems to support the idea of the chemical effect of additives, especially silica, on mechanical behaviour of the ceramics.[17] Whatever is the mechanism responsible for higher grain boundary strength, chemical, or mechanical, higher energy required for initiation of the transgranular fracture leads to higher wear resistance of both nanocomposites and liquid phase-sintered aluminas. The effect is more pronounced in materials with SiC nanoinclusions, than in those containing only C particles, being highest in liquid phase-sintered aluminas containing SiC/C nanoparticles.

The discussion above gives us some hints as to the ranking of wear resistance of materials of the Group 1. Taking into account

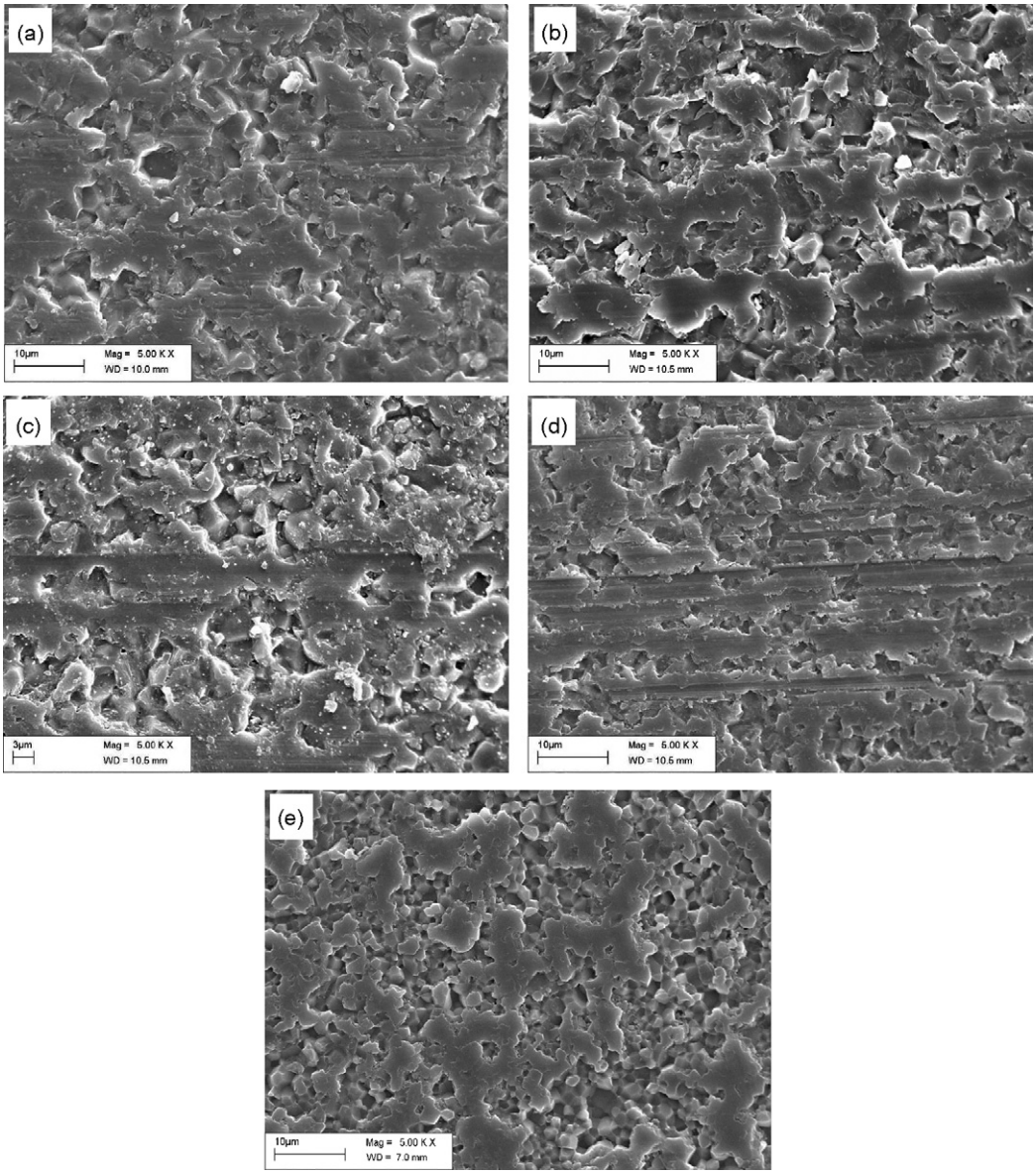

Fig. 9. Ground surfaces of nanocomposites IP3 (a, 3 vol% SiC), IP5 (b, 5 vol% SiC), IP8 (c, 8 vol% SiC), and IP8HIP (d, 8 vol% SiC, after HIP). The wear surface of the reference monolithic alumina T2 (e).

different wear controlling mechanism (grain pull-out in case of TGFS and T1, plastic grooving in other specimens), we suggest that the observed grain size dependence of wear within the Group 1 shown in Fig. 6 is of only limited significance, or it is only accidental. The addition of glass forming additives in TCS5 and TCS5G increased the wear resistance. We believe the reason is a chemical interaction of silicate grain boundary phase with alumina matrix grains, which increases the grain boundary strength. Our previous works with calcium and magnesium silicate containing aluminas confirmed their high resistance against wet and dry erosion, which was much higher than in monolithic alumina.[17,28] The highest wear resistance observed in liquid phase-sintered nanocomposite TCS5G is the result of synergy of two effects: chemical interaction of silicate phases with alumina matrix grains, and the grain boundary strengthening hydrostatic thermal residual stresses of SiC nanoparticles always located, due to very fine size of the alumina matrix grains, in a close vicinity of grain boundaries.

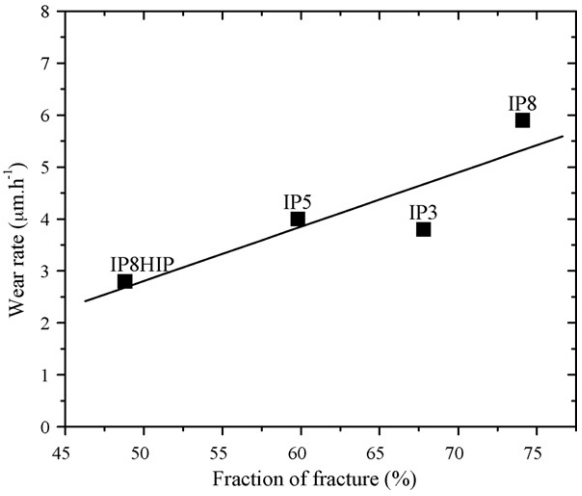

Fig. 10. Wear rate vs. the fraction of the sum of inter- and intra-granular fracture from image analysis of wear surfaces of nanocomposites with matrix grains >1 μm.

3.3. Group 2 materials with micrometer-sized alumina matrix grains

The materials in Group 2 consisted of coarser alumina matrix grains, with the mean diameter of around 2 μm for the monolithic alumina T2, samples IP5 and IP8, and 4 μm for the sample IP3. The SiC particles in IP3 were mainly located within the alumina grains: the fraction of inclusions in intergranular positions increased with increasing volume fraction of SiC[29] (Fig. 8 and Table 2). In contrast to the materials of Group 1, no obvious relationship between the wear rate and matrix grain size was observed, Table 2. In the contrary: despite of similar grain size a range of materials including the monolithic alumina T2 and "nanocomposites" with various volume fraction of SiC wore at very different rates.

Fig. 9 shows the wear surfaces of coarse-grained materials of Group 2 generated under the same grinding conditions as in the Group 1. The monolithic alumina (sample T2) exhibits typical features characteristic for intergranular fracture and grain pull-out as the results of coalescence of intergranular microcracks. In this respect the material T2 behaves similarly to monolithic aluminas of the Group 1, only the extent of grain pull-out is larger, and the damage correspondingly more severe.

All the composite materials of Group 2 exhibit mixed wear mode, where both the inter- and intra-granular fracture, and plastic grooving are in operation. In general, grain fracture and pull-out occurs as the major mode with no apparent dependence on the SiC content. However, a meticulous image analysis show that, upon decreasing the SiC content, enhanced amount of plastic deformation and the reduction of both the intra- and intergranular fracture are observed as the wear rate of the materials decreases (Fig. 10). This effect we attribute to two competing mechanisms: (I) grain boundary weakening by intergranular SiC particles as suggested by Ferroni et al., which gradually decreases with decreasing SiC content,[30] and (II) homogenization of the stress field and blocking of formation of long twins and dislocation pileups responsible for crack initiation by intragranular SiC particles.[16] Although Todd concludes that this mechanism can be effectively in operation only in composites with high fraction of SiC (>10 vol%), homogeneous distribution of large number of small intragranular SiC particles with small interparticle spacing in the IP3, Fig. 8, suggests possible contribution of the mechanism also in this case.

The only exception is the specimen IP8HIP, which wears markedly slower than one could expect on the basis of its microstructure, or SiC content, and stands quite outside the trends observed for the other Group 2 materials. This material exhibits the lowest area fraction of fracture and the highest proportion of plastic deformation in the wear surface. The HIP resulted only in slight decrease of the residual porosity: there seems therefore unlikely that such small decrease of porosity could have such profound influence on wear. Some hints were deduced from determination of thermal residual stresses by measuring the shift and broadening of photoluminescence peaks at polished cross-sections of both HIP-ed and un-HIP-ed specimens. The average negative (blue) R2 peak shift in both specimens was approximately 1 cm^{-1}. The blue shift reflects significant effect of SiC inclusions on the stress state in the material. In polycrystalline alumina the net stress is zero (although the shift is not) with c-axis tension being balanced by *a*- and *m*-axis compression. However, with the SiC present the net stress in the alumina is no longer zero since around each SiC particle there is a radial compressive stress, but tensile hoop stresses.

The IP8 specimen, Fig. 11a, shows a narrow distribution of shifts and the R1 and R2 peaks are also narrow (width of R1 approximately 22 cm^{-1}). The peak width and peak height ratios are very consistent and are in the normal range. The stress map, Fig. 11b, shows mild contrast features with a characteristic size of 10–20 μm, which most likely reflect the presence of clusters of alumina grains with local preferred orientation. The average shift of the IP8HIP specimen is very similar to that of IP8, but the details are very different. The histogram of shifts shows a much wider distribution (with some being as large as 2 cm^{-1}) indicating greater variability in the residual stress (Fig. 11c). The

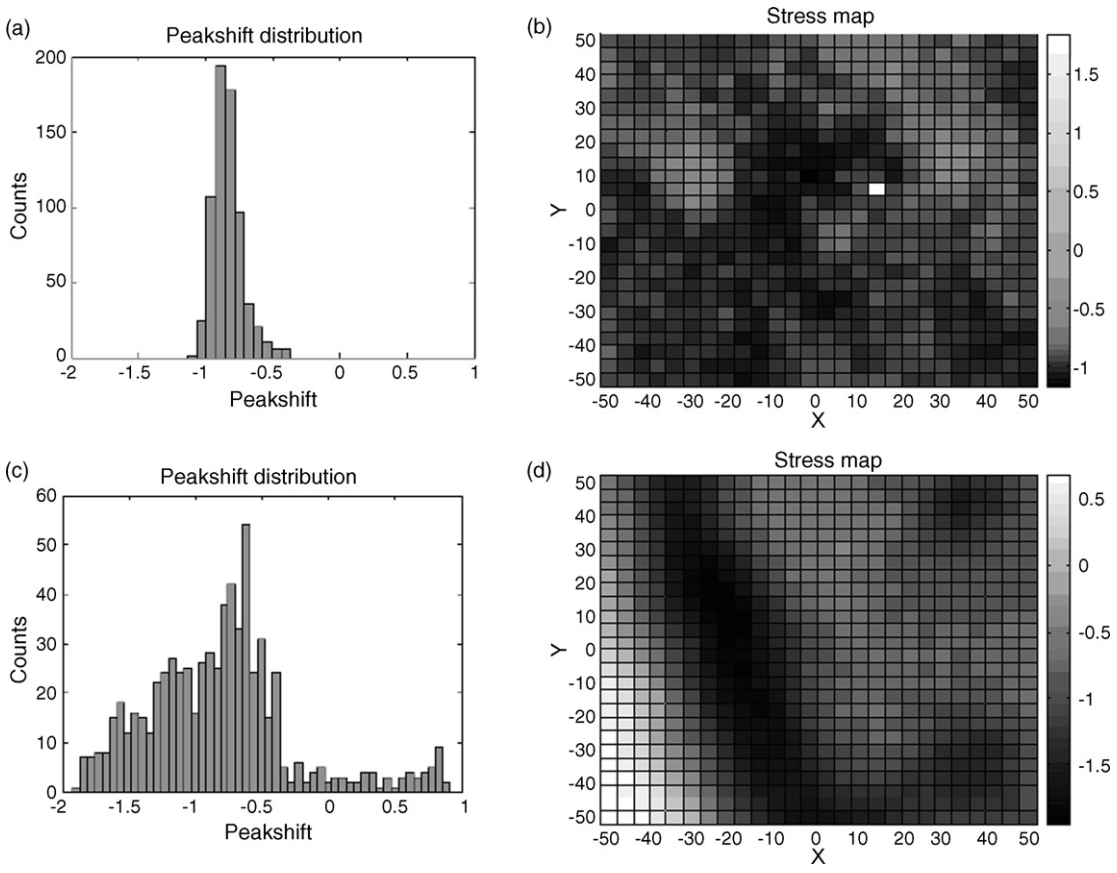

Fig. 11. The peak shift distributions and shift maps of the IP8 (a and b) and IP8HIP (c and d) samples. The units for peak shift are cm^{-1} and for the *X* and *Y* scales of the maps are μm.

individual peaks are significantly broader (typically 30 cm^{-1} for R1) indicating a larger spread of microstresses within each probed analysis volume, possibly due to a larger accumulation of dislocations. All the maps of the different parameters show broad linear contract features in which the shift (stress) is higher than elsewhere. Such high local stress levels together with accumulation of dislocations and densely interspersed intragranular SiC particles prevent the formation of long twins responsible for intragranular cracking, and promote plastic grooving as the principal mechanism of wear of the HIP-ed nanocomposite.

4. Summary

Even a qualitative interpretation of wear behaviour of alumina-based "nanocomposites" is not a trivial matter and a range of parameters has to be considered, including the volume fraction, size and location of nanoparticles, thermal expansion, and elastic modulus mismatch but also chemical interactions between the alumina matrix grains and a silicate grain boundary phase. According to their response to abrasion the studied materials could be divided into two groups: (1) materials with the submicrometer alumina matrix grains and high wear resistance and (2) materials with coarser alumina matrix grains (>1 μm), which wear comparatively faster.

The monolithic solid state-sintered aluminas of both groups respond to grinding predominantly by intergranular fracture and grain pull-out. The nanocomposites of the Group 1 wear predominantly by plastic grooving. The liquid phase-sintered monolithic alumina with silicate grain boundary phases behave similarly to nanocomposites of comparable grain size.

The nanocomposites of the Group 2 wear by inter- and intra-granular fracture combined with plastic deformation and grooving. The low wear rate is observed in composites with lower volume fraction of mainly intragranularly located SiC, and is correlated with higher extent of plastic grooving. Nanocomposites with higher volume fractions of SiC, and larger number of grain boundary wedging SiC particles, wear comparatively faster. A significant influence of the specimen stress state on its wear behaviour has been demonstrated on the case of the 8 vol% SiC nanocomposite before and after HIP.

Acknowledgements

The financial support of this work by the NATO Science for Peace Programme, under the contract No. SfP-981770, the Slovak National Grant Agency VEGA, grant No. 2/6181/26 is gratefully acknowledged. D. Galusek wishes to acknowledge the financial support of the Alexander von Humboldt Foundation. The authors wish to express their gratitude to M. Liška from SGAC Turnov, Czech Republic, for preparation of granulated powders, and Richard Todd from the Oxford University for valuable comments and discussion.

References

1. Miranda-Martinez, M., Davidge, R. W. and Riley, F. L., Grain size effects on the wet erosive wear of high-purity polycrystalline alumina. *Wear*, 1994, **172**, 41–48.
2. Davidge, R. W. and Riley, F. L., Grain-size dependence of the wear of alumina. *Wear*, 1995, **186–187**, 45–49.
3. Stachowiak, G. W. and Stachowiak, G. B., Wear behaviour of ceramic cutting-tools. *Key Eng. Mater.*, 1994, **96**, 137–164.
4. Walker, C. N., Borsa, C. E., Todd, R. I., Davidge, R. W. and Brook, R. J., Fabrication, characterisation and properties of alumina matrix nanocomposites. *Br. Ceram. Proc.*, 1994, **53**, 249–264.
5. Davidge, R. W., Twigg, P. C. and Riley, F. L., Effect of silicon carbide nanophase on the wet erosive wear of polycrystalline alumina. *J. Eur. Ceram. Soc.*, 1996, **16**, 799–802.
6. Anya, C. C., Wet erosive wear of alumina and its composites with SiC nano-particles. *Ceram. Int.*, 1998, **24**, 533–542.
7. Rodriguez, J., Martin, A., Pastor, J. Y., Llorca, J., Bartolome, J. F. and Moya, J. S., Sliding wear of alumina/silicon carbide nanocomposite. *J. Am. Ceram. Soc.*, 1999, **82**, 2252–2254.
8. Zhao, J., Stearns, L. C., Harmer, M. P., Chan, H. M., Miller, G. A. and Cook, R. F., Mechanical behavior of alumina–silicon carbide "nanocomposites". *J. Am. Ceram. Soc.*, 1993, **76**, 503–510.
9. Kara, H. and Roberts, S., Polishing behavior and surface quality of alumina and alumina/silicon carbide nanocomposites. *J. Am. Ceram. Soc.*, 2000, **83**, 1219–1225.
10. Sternitzke, M., Dupas, E., Twigg, P. and Derby, B., Surface mechanical properties of alumina matrix nanocomposites. *Acta Mater.*, 1997, **45**, 3963–3973.
11. Niihara, K., New design concept of structural ceramics, ceramic nanocomposites. *J. Ceram. Soc. Jpn.*, 1991, **99**, 974–982.
12. Levin, I., Kaplan, W. D., Brandon, D. G. and Layyous, A. A., Effect of SiC submicrometer particle size and content on fracture toughness of alumina–SiC nanocomposites. *J. Am. Ceram. Soc.*, 1995, **78**, 254–256.
13. Winn, A. J. and Todd, R. I., Microstructural requirements for alumina–SiC nanocomposites. *Br. Ceram. Trans.*, 1999, **98**, 219–224.
14. Xu, Y., Zangvil, A. and Kerber, A., SiC nanoparticle-reinforced Al_2O_3 matrix composites: role of intra- and intergranular particles. *J. Eur. Ceram. Soc.*, 1997, **17**, 921–928.
15. Luo, J. and Stevens, R., The role of residual stresses on the mechanical properties of Al_2O_3–5 vol% SiC nanocomposites. *J. Eur. Ceram. Soc.*, 1997, **17**, 1565–1572.
16. Todd, R. I. and Limpichaipanit, A., Microstructure-property relationships in wear resistant alumina/SiC nanocomposites. *Adv. Sci. Technol.*, 2006, **45**, 555–563.
17. Galusek, D., Kido, L., Pánek, Z., Lenčéš, Z., Šajgalík, P. and Riley, F. L., The influence of sintering additives on fracture behaviour and wear of liquid phase sintered polycrystalline alumina. *Key Eng. Mater.*, 2002, **223**, 227–232.
18. Moraes, K. V. and Interrante, L. V., Processing, fracture toughness, and Vickers hardness of allylhydridopolycarbosilane-derived silicon carbide. *J. Am. Ceram. Soc.*, 2003, **86**, 342–346.
19. Anstis, G. R., Chantikul, P., Lawn, B. R. and Marshall, D. B., A critical evaluation of indentation techniques for measuring fracture toughness. I. Direct crack measurement. *J. Am. Ceram. Soc.*, 1981, **64**, 533–538.
20. Evans, A. G. and Marshall, D. B., Wear mechanisms in ceramics. In *Fundamentals of Friction and Wear of Materials*, ed. D. A. Rigney. American Society for Metals, Metals Park, OH, 1981, pp. 439–452.
21. Xu, H. H. K., Jahanmir, S. and Wang, Y., Effect of grain size on scratch interactions and material removal in alumina. *J. Am. Ceram. Soc.*, 1995, **78**, 881–891.
22. Cho, S.-J., Hockey, B. J., Lawn, B. R. and Bennison, S. J., Grain-size and *R*-curve effects in the abrasive wear of alumina. *J. Am. Ceram. Soc.*, 1989, **72**, 1249–1252.
23. Roberts, S. G., Depths of cracks produced by abrasion of brittle materials. *Scripta Mater.*, 1999, **40**, 101–108.
24. Sedláček, J., Galusek, D. and Švančárek, P., Alumina–carbon composites with high hardness. *Key Eng. Mater.*, 2004, **264–268**, 841–844.
25. Blendell, J. E. and Coble, R. L., Measurement of stress due to thermal expansion anisotropy in Al_2O_3. *J. Am. Ceram. Soc.*, 1982, **65**, 174–178.
26. Barceinas-Sanchez, J. D. O. and Rainforth, W. M., On the role of plastic deformation during the mild wear of alumina. *Acta Mater.*, 1998, **46**, 6475–6483.
27. Todd, R. I. and Derby, B., Thermal stress induced microcracking in alumina–20% SiCp composites. *Acta Mater.*, 2004, **52**, 1621–1629.
28. Galusek, D., Brydson, R., Twigg, P. C., Riley, F. L., Atkinson, A. and Zhang, Y.-H., Wet erosive wear of alumina densified with magnesium silicate additions. *J. Am. Ceram. Soc.*, 2001, **84**, 1767–1776.
29. Galusek, D., Čierniková, E. and Riedel, R., Final-stage sintering of polymer-derived Al_2O_3–SiC nanocomposites. In *Proceedings of the Fourth International Conference on Science, Technology and Applications of Sintering, Sintering' 05*, 2005, pp. 106–109.
30. Ferroni, L. P. and Pezzotti, G., Evidence for bulk residual stress strengthening in Al_2O_3/SiC nanocomposites. *J. Am. Ceram. Soc.*, 2002, **85**, 2033–2038.